Supplementary Methods

Cell Culture

The human hepatoma cell line HuH-7[1] and its derivative cell line Huh-7.5.1[2] were maintained in Dulbecco's modified Eagle medium supplemented with 10% fetal bovine serum, minimal essential medium nonessential amino acids, 100 U/mL penicillin, 100 μg/mL streptomycin, 10 mM HEPES, and 1 mM sodium pyruvate at 37°C in a 5% CO_2 incubator.

Primary human hepatocytes (PHH) were isolated from an encapsulated liver sample.[3] Isolated PHH were seeded in 12-well plates and cultured at 37°C in Lanford medium before infection.

PHH Infection With HCV-Positive Sera

Three days post seeding, PHH were inoculated with HCV-positive sera. After 16 h of inoculation, monolayers were washed with William's E medium and fresh Lanford medium was added. Cells were harvested at 72 h post infection. Total RNA was isolated using a guanidinium isothiocyanate solution (RNAble; Eurobio, Courtaboeuf, France) and intracellular levels of HCV RNA were quantified using the SuperScript III Platinium One-Step quantitative reverse transcription polymerase chain reaction (RT-PCR) system (Invitrogen, Carlsbad, CA) and a LightCycler480 real-time PCR system (Roche Diagnostics, Meylan, France).

HCV Genotype 3a Clone

Clone S310 was isolated from a 71-year-old female patient suffering from post liver transplantation HCV recurrence. She was diagnosed with HCV genotype 3a infection at the age of 59 years and underwent liver transplantation 4 years later due to liver cirrhosis. HCV-RNA titer was 2.8×10^6 copies/mL. Total RNA extracted from 100 μL serum using the acid-guanidinium isothiocyanate-phenol-chloroform method (Isogen-LS; Nippon Gene, Tokyo, Japan) was precipitated with isopropanol, washed with ethanol, and dissolved in 10 μL nuclease-free water. An aliquot of 4 μL was subjected to reverse transcription using random hexamers and Moloney murine leukemia virus reverse transcriptase (Superscript III; Invitrogen) at 42°C for 50 min and then at 50°C for 10 min.

Isolation of HCV

The sequences of 4 isolates of genotype 3a (accession numbers AF046866, D28917,[4] X76918, and D17763[5]) that were obtained from the HCV database (http://hcv.lanl.gov/content/sequence/HCV/ToolsOutline.html) were aligned and PCR primers were designed based on the conserved sequences. These primers were used to amplify the complementary DNA (cDNA) of S310 into 9 overlapping fragments by nested PCR (nt 1–370, nt 127–1284, nt 1117–1997, nt 1704–3352, nt 3152–5080, nt 4869–6842, nt 6601–8129, nt 7988–9145, and nt 9082–9576; nucleotide numbers refer to the positions on S310, with nt 1 being the first nucleotide of the 5′ UTR). The sequence of these primers is shown in Supplementary Table 1. Two microliters of cDNA was subjected to PCR using Pyrobest DNA polymerase (Takara Bio, Kyoto, Japan) and the outer set of primers, and this first-round PCR product (2 μL) was further amplified by a second round of PCR using the inner set of primers. PCR conditions for the first and second rounds of PCR consisted of 35 cycles each of denaturation at 98°C for 20 s, annealing at 55°C for 1 min, and extension at 72°C for 3 min. A fragment encompassing the 5′ end of the viral genome (nt 1–370) was amplified by 5′RACE. Briefly, cDNA was synthesized with a 5′ UTR primer (antisense), tailed with a dCTP homopolymer by using terminal deoxynucleotidyl transferase, and amplified by PCR (5′ RACE System for Rapid Amplification of cDNA Ends; Invitrogen) using TaKaRa LA Taq polymerase (Takara Bio). The PCR products of all fragments were separated by agarose gel electrophoresis, cloned into the pGEM-T EASY vector (Promega, Madison, WI) and sequenced using the Big Dye Terminator Mix and an automated DNA sequencer. The consensus sequence of 5 to 9 isolated cDNA clones was adopted for each fragment. Two major populations of the virus were identified in the patient's serum that differed in 4 amino acids in the NS3 protein (aa 1039, 1183, 1463, and 1504), and these populations were designated as S310/A and S310/B (DDBJ/EMBL/GenBank accession number: AB691595 and AB691596, respectively). To assess the complexity of the HCV population in the patient's serum, the hypervariable region sequences of 10 clones were determined.

Computer Analysis

A phylogenetic tree was constructed using the neighbor-joining method to examine the relationship between the polyprotein region of S310 and that of other HCV genotype 3a isolates available in the database. In order to analyze the diversity in each subgenomic region, the genetic distance was calculated between all possible pairs of genotype 3a isolates and between S310/A and other isolates using MacVector software (MacVector, Inc., Cary, NC). The ratios of these 2 values (mean genetic distance between S310/A and other isolates/mean genetic distance among all genotype 3a isolates) were compared.

Construction of Replicons

Based on the consensus sequence of S310, we assembled pS310/A and pS310/B, which contained the full-length S310/A and S310/B cDNA, respectively, downstream of the T7 RNA polymerase promoter. Briefly the 9 amplicons described here were combined by overlapping PCR and ligated with pGEM-T EASY vectors to generate 6 plasmids (A through F) in such a way that each plasmid contained a unique restriction enzyme

cleavage site toward the 3′ end of the viral fragment, which overlapped with the 5′ end of the next fragment. For this purpose, we took advantage of the EcoRI restriction site that is present in the polycloning site of the plasmid toward the 5′ end of the viral fragment. Plasmid A contained the T7 promoter sequence followed by one G-nucleotide and nt 1–3352 of S310, while plasmids B, C, D, and E contained nt 1704–4307, nt 4044-6013, nt 5424–7755, and nt 7276–9425, respectively. Plasmid F contained the fragment constructed by combining the C-terminal end of NS5B (nt 9182–9402) and the variable and poly U/UC regions of the S310/A 3′UTR (nt 9403–9610) with the last 44 nucleotides of JFH-1. Restriction sites for EcoRI and XbaI were introduced upstream of the T7 promoter sequence and downstream of the conserved region, termed the *X-region*, of the 3′UTR, respectively, and the restriction sites of these enzymes that were present within the cDNA were removed by PCR-based mutagenesis. In the neomycin-based subgenomic replicons (SGR-S310/A and SGR-S310/B, accession number: AB691597 and AB691598, respectively), the cassette containing the neomycin phosphotransferase gene and the EMCV IRES replaced the region of S310 that encompasses amino acids 20–1032. Firefly luciferase–based subgenomic replicons (SGR-S310/Luc, accession number: AB691599) were generated from SGR-S310/A by replacing amino acids 20–1032 of S310/A with the cassette containing firefly luciferase and the EMCV IRES from pSGR-JFH1/Luc.[6]

RNA Synthesis

RNA was synthesized by in vitro transcription as described previously.[7] Briefly, the plasmids carrying the cDNA described here were linearized with the XbaI restriction enzyme and 5′ overhangs were removed by treating with mung bean nuclease. Reaction mixtures were further incubated at 50°C for 1 h with 2 μL 20 mg/mL proteinase K and 10 μL 10% sodium dodecyl sulfate to degrade nucleases, and templates were purified with 2 rounds of phenol-chloroform extraction and ethanol precipitation. Three micrograms of templates were subjected to in vitro transcription using a MEGAscript T7 kit (Ambion, Austin, TX) according to the manufacturer's recommendations. Synthesized RNA was treated with DNase I (Ambion) and then purified using ISOGEN-LS (Nippon Gene). The quality of the synthesized RNA was examined by agarose gel electrophoresis.

RNA Transfection

In vitro transcribed RNA or total cellular RNA isolated from replicon cells was introduced into cells by electroporation. Trypsinized cells were washed twice with serum-free Opti-MEM I (Invitrogen) and 3.0×10^6 cells were resuspended in 400 μL cytomix buffer.[8] RNA was delivered into cells by a single pulse of 260 V and 950 μF using the Bio-Rad Gene Pulser II apparatus (Bio-Rad, Hercules, CA). Transfected cells were immediately suspended in culture medium and transferred to the appropriate plates. For G418 selection of colonies, the transfected cells were seeded in 10-cm dishes, each containing 8 mL culture medium. G418 (500 μg/mL; Nacalai Tesque, Kyoto, Japan) was added to the culture medium at 24 h after transfection. Culture medium supplemented with G418 was replaced every 3 days. Three weeks after transfection, cells were fixed with buffered formalin and stained with crystal violet or replicon colonies were picked and expanded.

Analysis of G418-Resistant Cells

G418-resistant colonies were collected and used for further analysis. Colonies were independently isolated using cloning cylinders (Asahi Techno Glass Co., Tokyo, Japan) and were expanded until they were 80%–90% confluent in 10-cm dishes. Expanded cells were harvested for nucleic acid and protein analysis. Total RNA was isolated from the cells using the ISOGEN reagent (Nippon Gene). Another aliquot of the cell pellet was dissolved in RIPA buffer containing 0.1% sodium dodecyl sulfate for Western blot analysis. For immunofluorescence analysis of viral proteins, cells were seeded on 12-well slides.

Quantification of HCV RNA by Real-Time RT-PCR

Copy numbers of HCV RNA were determined by real-time detection RT-PCR, as described previously,[9] using the ABI Prism 7700 Sequence Detector System (Applied Biosystems Japan, Tokyo, Japan). The concentration of total RNA in the cells was determined using a Nanodrop Spectrophotometer ND-1000 (Thermo Scientific, Rockford, IL).

Northern Blot Analysis

Isolated RNAs (3 μg) from replicon cells were separated on a 1% agarose gel containing formaldehyde, transferred to a positively charged nylon membrane (Hybond-N+; GE Healthcare UK Ltd., Buckinghamshire, UK) and immobilized using a FUNA-UV-LINKER (Funakoshi, Tokyo, Japan). Hybridization was carried out with a [α-^{32}P]dCTP-labeled DNA probe using Rapid-Hyb buffer (GE Healthcare UK Ltd.). The DNA probe was synthesized from a BsrGI-MfeI fragment of the S310 clone that contained NS3-5B genes using the Megaprime DNA labeling system (GE Healthcare UK Ltd.).

Indirect Immunofluorescence

Untransfected HuH-7 cells or S310 replicon-replicating cells were grown on a glass slide for 24 h and fixed in acetone-methanol (1:1 [vol/vol]) for 10 min at −20°C. Cells were then incubated in immunofluorescence buffer (phosphate-buffered saline, 1% bovine serum albumin, 2.5 mM EDTA). S310 patient serum was added at

a dilution of 1:200 in immunofluorescence buffer. After incubation for 1 h at room temperature, cells were washed and then incubated with an Alexa Fluor488–conjugated goat anti-human IgG antibody (Invitrogen) in immunofluorescence buffer. The glass slide was washed and a cover glass was mounted using PermaFluor mounting solution (Thermo Scientific, Cheshire, UK). Cells were examined under a fluorescence microscope (Olympus, Tokyo, Japan).

Western Blot Analysis of HCV Proteins

The protein samples were separated on 12.5% polyacrylamide gels and subsequently transferred to a polyvinylidene difluoride membrane (Immobilon; Millipore, Bedford, MA). Transferred proteins were incubated with 2% skim milk. Anti-NS3 mouse monoclonal antibody (clone 8G2, Abcam, Cambridge, UK) and peroxidase-labeled sheep anti-mouse IgG (Cell Signaling Technology, Danvers, MA) were used to detect HCV proteins. The signals were detected with a chemiluminescence system (ECL Prime; GE Healthcare UK Ltd.).

Identification of Mutations

cDNA was synthesized from total RNA that was extracted from replicon-expressing cells at 2 different times. These cDNAs were amplified into 5 overlapping fragments that spanned the 5′UTR and the NS3-NS5B region using LA Taq DNA polymerase (Takara Bio) and the primers described in Supplementary Table 1. The sequence of each amplified DNA was determined. The mutations identified were subsequently introduced into SGR-S310/A and SGR-S310/Luc by PCR-mediated mutagenesis.

Luciferase Assay

Five micrograms of RNA, prepared by in vitro transcription of S310/SG-FLuc constructs with or without adaptive mutations, were introduced into 3.0×10^6 Huh-7.5.1 cells by electroporation. Cells were harvested with Cell Culture Lysis Reagent (Promega) at 4, 24, 72, and 96 h post electroporation, and luciferase activity was determined by use of a Luciferase Assay System (Promega) and the Lumat LB9507 luminometer (EG & G Berthold, Bad Wildbad, Germany).

Inhibition of S310 Replicon Replication by Specific Inhibitors

S310 replicon cell clones 6, 9, and 10 and the genotype1b Con1 and 2a JFH-1 replicon cells,[10] were seeded into 24-well plates at a density of 5.0×10^4 cells/well. On the next day, the culture medium was replaced with medium containing 0.1% dimethyl sulfoxide with or without various concentrations of interferon alfa (Dainippon-Sumitomo, Osaka, Japan), the specific NS3 protease inhibitor, BILN-2061 (Boehringer Ingelheim Ltd., Québec, Canada), or the NS5B inhibitors, JTK-109 (Japan Tobacco, Inc., Osaka, Japan) and PSI-6130 (Pharmasset, Inc., Princeton, NJ). After 72-h incubation, cells were harvested and HCV RNA was quantified as described.

Supplementary References

1. Nakabayashi H, et al. Cancer Res 1982;42:3858–3863.
2. Zhong J, et al. Proc Natl Acad Sci U S A 2005;102:9294–9299.
3. Pichard L, et al. Methods Mol Biol 2006;320:283–293.
4. Yamada N, et al. J Gen Virol 1994;75:3279–3284.
5. Sakamoto M, et al. J Gen Virol 1994;75:1761–1768.
6. Kato T, et al. J Clin Microbiol 2005;43:5679–5684.
7. Wakita T, et al. Nat Med 2005;11:791–796.
8. van den Hoff MJ, et al. Nucleic Acids Res 1992;20:2902.
9. Takeuchi T, et al. Gastroenterology 1999;116:636–642.
10. Miyamoto M, et al. Intervirology 2006;49:37–43.

Supplementary Table 1. Primers for Amplification of the S310 HCV Strain

	Fragment		Primer sequence (5′→3′)
1 (5′ RACE)[a]	Outer	Antisense	CTTGACGTCCTGTGGGCGA
	Inner	Antisense	TTTTTCTTTGGGGTTTAGG
2	Outer	Sense	GTCTTCACGCGGAAAGCGC
		Antisense	CACCCAAACCACCGACCAC
	Inner	Sense	CCGGGAGAGCCATAGTGGTC
		Antisense	TCCTGAAAGATGGCCTGGGTA
3	Outer	Sense	CTTGGCCCCTCTATGGTAA
		Antisense	GATGTTTCCTGAAGCAGTCG
	Inner	Sense	AGTCATGTGGACCTATTAGT
		Antisense	CACCCAAACCACCGACCAC
4	Outer	Sense	ATGGCTCGTGGCACATCAA
		Antisense	TAGTCATCAGCAGGTCCCAA
	Inner	Sense	GCTCAGCAGCTGCAAGCCCAT
		Antisense	CGCAAAGAATATCTCCGCAAG
5	Outer	Sense	ATTTTTGACATCACTAAGCTAC
		Antisense	AGTGTTGGCTTAAGCCGCA
	Inner	Sense	AATACTTCCAGATGATCATACT
		Antisense	GTGACAGAAAGTGGGCAT
6	Outer	Sense	GTTTCCCGCAGCCAACGT
		Antisense	GTCTCTCAACATCGAGGT
	Inner	Sense	CGGTGAAAGACCGTCTGGA
		Antisense	CAGGGGAGTTGAGATCCT
7	Outer	Sense	GGCCGCGTACATGTGCTAAC
		Antisense	CCGCAGACAAGAAAGTCCGGGT
	Inner	Sense	CTATGGCGCGTGGCTGCCA
		Antisense	ACCCCCAGGTCAGGGTACAC
8	Outer	Sense	CATAACCTAGTCTATTCAACG
		Antisense	TGGTCTTGGTGCGTACCG
	Inner	Sense	GCTCCGTCTGGGAGGACTTGC
		Antisense	CTCGTGCCCGATGTCTCCAA
9	Outer	Sense	TGCTCCTCCAACGTCTCCGT
		Antisense	GCGGCTCACGGACCTTTCAC
	Inner	Sense	GTCGCGGGGACACTCAGGAA
		Antisense	ACTAGGGCTAAGATGGAGCC

RACE, rapid amplification of complementary DNA ends.

[a]Forward primers used were those in the 5′RACE kit (Abridged Universal Amplification Primer (AUAP) for the first round of PCR and Universal Amplification Primer (UAP) for the second round of PCR).

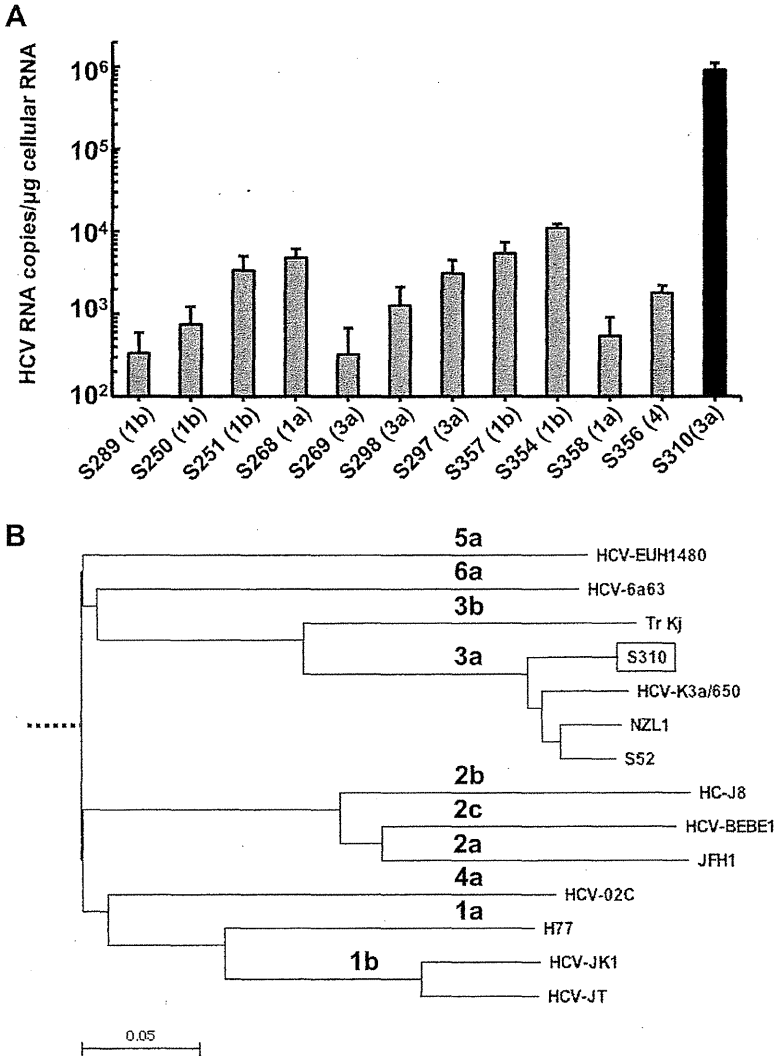

Supplementary Figure 1. Infection of PHH with HCV patient sera and phylogenetic tree analysis of the S310 strain. (*A*) PHH were exposed to sera of patients infected with genotype 1b (S289, S250, S251, S357, S354), 1a (S268, S358), 3a (S269, S298, S297, S310), and 4 (S356) for 16 h (25 µL/well, except for S310, 10 µL). Intracellular HCV RNA was quantified 72 h post inoculation. Experiments were done in triplicate and data are presented as means ± standard deviation. (*B*) The phylogenetic tree was constructed using the polyprotein region of S310 and HCV strains of different genotypes. The HCV strains analyzed and their corresponding GenBank accession numbers are: K3a/650; D28917, NZL1; NC_009824, S52; GU814263, EUH1480, HCV-6a63; DQ480514, Tr Kj; D49374, HC-J8; D10988, BEBE1; D50409, JFH-1; AB047639, HCV-02C; DQ418784, H77; AF009606, HCV-JK1; X61596 and HCV-JT; D11168. The root of the tree was tentatively taken as the midpoint of the longest path. The length of the horizontal bar indicates the number of nucleotide substitutions per site.

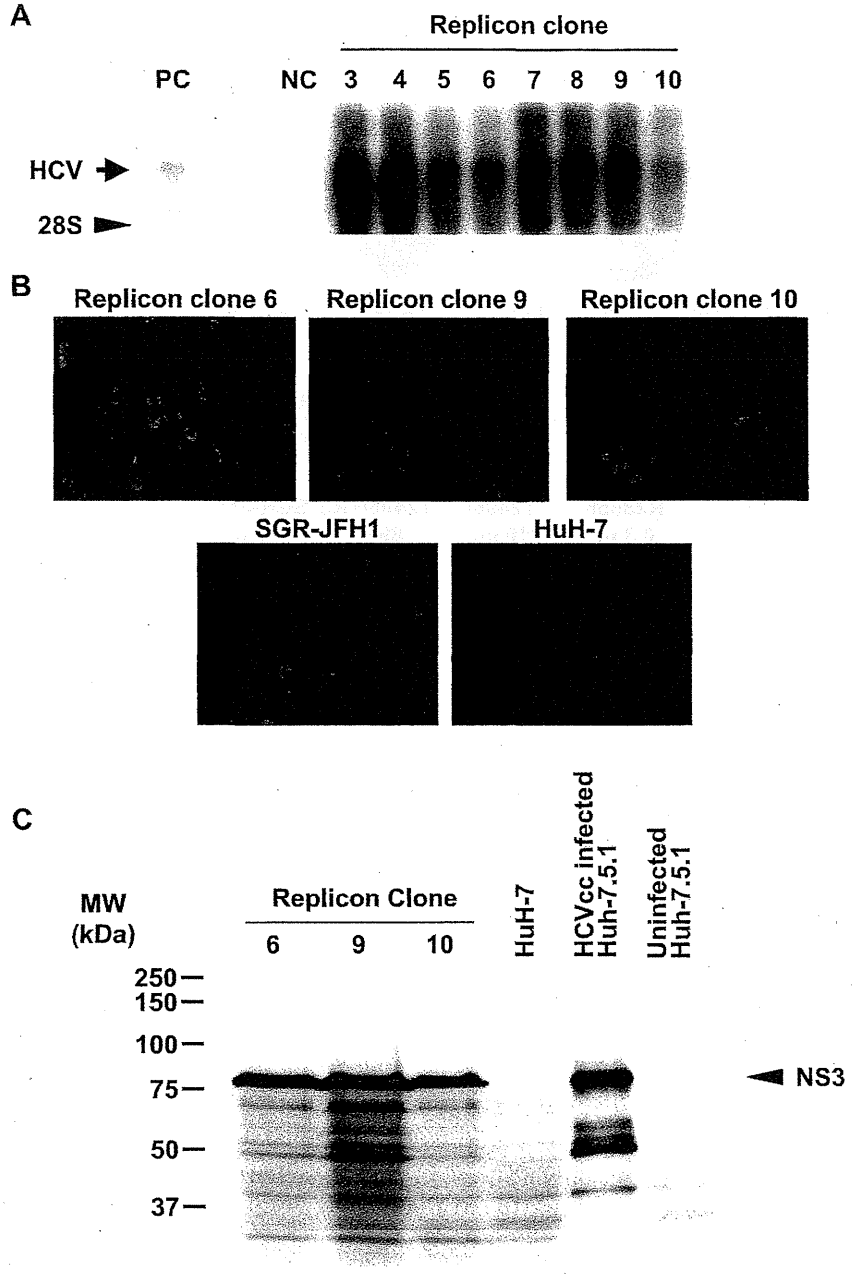

Supplementary Figure 2. Detection and quantification of HCV RNA and proteins in replicon cells. (*A*) Total RNA (3 μg) from replicon cells was analyzed by Northern blot; 5.0×10^7 copies of in vitro–transcribed RNA were loaded in parallel as a positive control (PC), while total RNA from untransfected HuH-7 cells served as the negative control (NC). Replicon RNA was detected using a [α-^{32}P]dCTP-labeled DNA probe. Arrow and arrowhead indicate the positions of the replicon RNA and 28S ribosomal RNA, respectively. (*B*) Subcellular localization of viral proteins determined by immunofluorescence. S310 replicon cell clones, JFH-1 replicon cells, and untransfected HuH-7 cells were grown on glass slides for 24 h. After fixation, cells were incubated with patient serum. (*C*) Western blot analysis. Cell lysates were prepared from replicon clones 6, 9, and 10, untransfected HuH-7, and HCVcc (J6/JFH1)-infected Huh-7.5.1 cells and uninfected Huh-7.5.1 cells. Protein (10 μg) was resolved by 12.5% sodium dodecyl sulfate polyacrylamide gel electrophoresis and viral nonstructural protein NS3-specific bands were detected using an anti-NS3 mouse monoclonal antibody (clone 8G2). Arrow indicates the position of NS3.

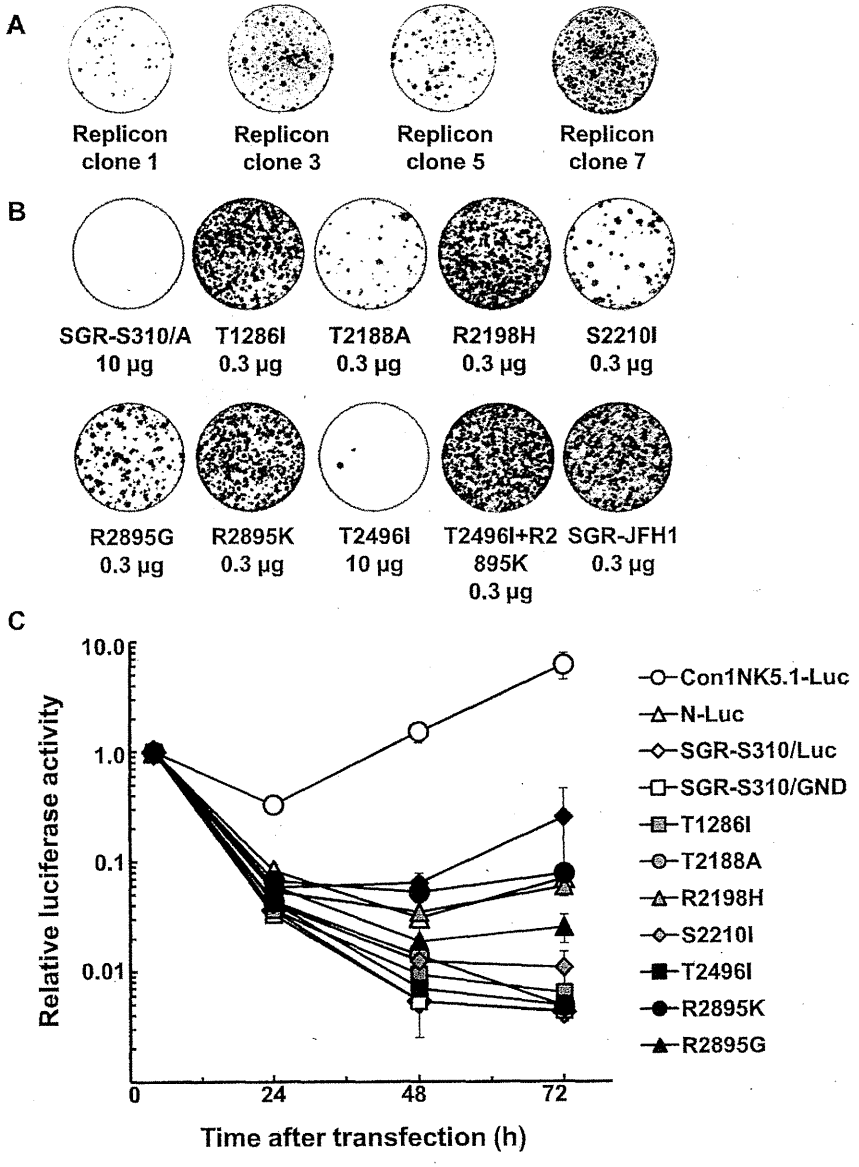

Supplementary Figure 3. Analysis of the effect of mutations on the colony-forming efficiency and transient replication of the subgenomic replicon S310. (*A*) Total RNA was isolated from the indicated replicon cell clones and 10 µg RNA was introduced into 3 million naïve HuH-7 cells by electroporation. After 3 weeks of G418 selection (500 µg/mL), colonies were stained. (*B*) Three million HuH-7 cells were electroporated with the indicated amounts of transcribed RNA and colonies were selected by a 3-week G418 selection. The JFH-1 subgenomic RNA was included as a positive control. (*C*) Huh-7.5.1 cells were transfected with the transcribed RNA from pSGR-S310/Luc and pSGR-S310/Luc constructs with mutations (GND mutation in NS5B, T1286I, T2188A, R2198H, S2210I, T2496I, R2895K, R2895G, and T2496I+R2895K) and Con1-NK5.1/Luc and N/Luc replicon. Transfected cells were harvested at the indicated time points and at 4 h post transfection. Relative luciferase activity (arbitrary units) was measured in the cell lysate and was normalized to the activity at 4 h post transfection. Assays were performed in triplicate, and data are presented as means ± standard deviation.

Genes to Cells

Interaction between RB protein and NuMA is required for proper alignment of spindle microtubules

Chiharu Uchida[1,2]*, Takayuki Hattori[2,3], Hirotaka Takahashi[4,5], Naoki Yamamoto[5], Masatoshi Kitagawa[1,6] and Yoichi Taya[2]

[1]*Research Equipment Center, Hamamatsu University School of Medicine, 1-20-1 Handayama, Higashi-ku, Hamamatsu, Shizuoka 431-3192, Japan*

[2]*Cancer Science Institute of Singapore (CSI-Singapore), National University of Singapore, Centre for Translational Medicine, 14 Medical Drive, #12-01, 117599, Singapore*

[3]*Division of Biochemistry and Molecular Biology, National Institute of Health Sciences, Kamiyoga 1-18-1, Setagaya-ku, Tokyo 158-8501, Japan*

[4]*Division of Cell-Free Sciences, Proteo-Science Center, Ehime University, 3 Bunkyo-cho, Matsuyama, Ehime 790-8577, Japan*

[5]*Department of Microbiology, Yong Loo Lin School of Medicine, National University of Singapore, Centre for Translational Medicine (MD6), 14 Medical Drive, 117599, Singapore*

[6]*Department of Molecular Biology, Hamamatsu University School of Medicine, 1-20-1 Handayama, Higashi-ku, Hamamatsu, Shizuoka 431-3192, Japan*

Retinoblastoma protein (pRB) controls cell cycle progression and cell cycle exit through interactions with cellular proteins. Many pRB-binding proteins, which function in gene transcription or modulation of chromatin structure, harbor LXCXE motifs in their binding domain for pRB. In this study, we found that nuclear mitotic apparatus protein (NuMA), a mitotic spindle organizer, interacts with pRB through LSCEE sequences located in its C-terminal region. siRNA-mediated down-regulation of pRB caused aberrant distribution of NuMA and alignment of spindle microtubules in mitotic cells. Abnormal organization of spindle microtubules was also accompanied by misalignment of an over-expressed NuMA mutant (mut-NuMA) with a defect in pRB binding caused by an LSGEK mutation. The mut-NuMA-over-expressing cells showed lower potency for survival than wild-type NuMA (wt-NuMA)-over-expressing cells during 2 weeks of culture. Interestingly, knockdown of pRB reduced the population of wt-NuMA-over-expressing cells to the same level as mut-NuMA cells after 2 weeks. Taken together, pRB may have a novel function in regulating the mitotic function of NuMA and spindle organization, which are required for proper cell cycle progression.

Introduction

Retinoblastoma protein (pRB) plays a major role in regulating G1-S progression through interaction with E2Fs by inhibiting E2F-dependent expression of cell cycle-related genes (Dyson 1998; Uchida 2012). It is generally recognized that the transcriptional regulation by pRB requires cooperation with pRB-interacting proteins. Many pRB-binding proteins contain LXCXE sequences as binding motifs for pRB. Through cooperation with pRB, these LXCXE-containing proteins have been shown to play important roles in nucleosome remodeling, stabilization, and organization of the higher-order structure of chromatin in the regulation of gene expression (Dahiya *et al.* 2000; Chan *et al.* 2001; Uchida 2012).

Recently, it was shown that pRB is also involved in the regulation of mitotic progression and chromosomal stability through controlling E2F-target gene expression (Schvartzman *et al.* 2011; Uchida 2012). It is known that pRB inactivation compromises mitotic progression by inducing centrosome hyperamplification and abnormal chromosomal condensation or segregation (Iovino *et al.* 2006; Manning *et al.* 2010). The effects of pRB inactivation on mitotic progression can be explained by failure in the inhibitory

Communicated by: Keiichi I. Nakayama
**Correspondence*: cuchida@hama-med.ac.jp

DOI: 10.1111/gtc.12119

regulation of E2F-dependent expression of mitotic genes, although direct involvement of pRB in mitosis has been proposed (van Deursen 2007; Alderton 2010).

Nuclear mitotic apparatus protein (NuMA) is abundantly present throughout the cell cycle and is known to be essential for spindle assembly and maintenance during M-phase (Radulescu & Cleveland 2010). For regulation of mitotic spindle assembly, NuMA cooperates with other spindle organizers, including Rae1 and LGN (Wong *et al.* 2006; Radulescu & Cleveland 2010). A recent study showed that Nup188 is also a binding partner of NuMA that participates in the regulation of chromosome alignment during mitosis (Itoh *et al.* 2013). NuMA is localized in the nucleus during interphase, but its role is not completely understood. It has been considered that interphase NuMA may form scaffolds for nucleocytoskeletal or chromatin proteins and regulate higher-order chromatin organization. Recent reports shown that NuMA acts as a member of a transcriptional regulator complex that induces p53-mediated expression of genes for cell cycle arrest (Endo *et al.* 2013; Ohata *et al.* 2013).

In this study, we identified an interaction between pRB and NuMA. Our findings support previous research on the contribution of pRB to mitosis and could provide a new insight into LXCXE-containing proteins.

Results

pRB interacts with NuMA

In a series of primary examinations, we noted that down-regulation of pRB induced aberrant alignment of spindle microtubules. This observation prompted us to examine whether pRB could interact with certain mitotic regulators to control their activities for the synthesis and/or alignment of spindle microtubules. By searching for such regulators with domains containing LXCXE motifs, a binding motif for pRB, we found that NuMA contains LSCEE sequences in its C-terminus (Fig. 1A). NuMA, a 238-kDa protein,

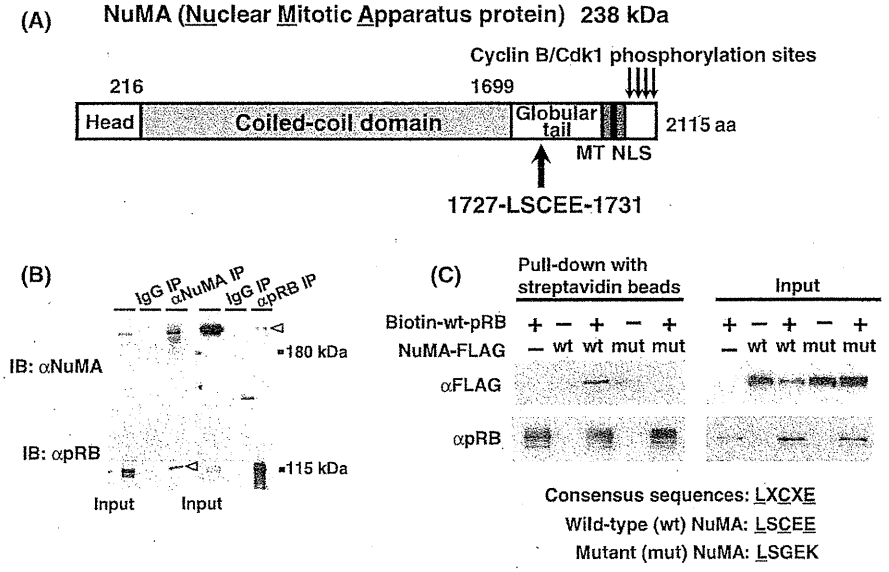

Figure 1 Interaction between retinoblastoma protein (pRB) and nuclear mitotic apparatus protein (NuMA). (A) Schematic representation of the NuMA molecule. The numbers of amino acid residues are indicated. MT: microtubule-binding domain (residues 1900–1971); NLS: nuclear localization signal (residues 1971–1991). The arrows indicate the cyclin B/Cdk1 phosphorylation sites. (B) Endogenous interaction between pRB and NuMA. Anti-pRB (αpRB) or anti-NuMA (αNuMA) antibodies were incubated with extracts of MOLT-4 cells in the presence of Dynabeads protein G, and the precipitated proteins were subjected to Western blotting analyses. The arrowheads indicate the coprecipitated pRB and NuMA. (C) Biotin-wt-pRB pulls down wt-NuMA-FLAG. *In vivo*-biotinylated pRB in MCF7-BirA cells transfected with NuMA-FLAG expression vectors was pulled down from the cell lysates with streptavidin beads. The precipitated proteins were analyzed by Western blotting using anti-FLAG (αFLAG) and anti-pRB (αpRB) antibodies.

is known to be essential for spindle assembly and maintenance during M-phase (Radulescu & Cleveland 2010). The NuMA molecule comprises globular head and tail domains separated by a coiled-coil region. The C-terminal globular tail contains a microtubule-binding domain and cyclin-dependent kinase 1 (Cdk1)-phosphorylation sites that contribute to tethering of microtubules for organization of spindle poles. To investigate whether pRB could bind to NuMA, we carried out immunoprecipitation analyses of endogenous proteins in MOLT-4 cells using specific antibodies against pRB and NuMA. As shown in Fig. 1B, endogenous NuMA and pRB coimmunoprecipitated with pRB and NuMA, respectively. We then examined the effects of mutations in the LSCEE sequences on the pRB–NuMA interaction. Wild-type NuMA-FLAG (wt-NuMA-FLAG) or mutant NuMA-FLAG (mut-NuMA-FLAG) containing LSGEK sequences, and biotinylated wild-type pRB (biotin-wt-pRB) were transiently co-expressed in MCF7-BirA cells. The biotin-wt-pRB was then pulled down from the cell lysates with streptavidin beads. Wt-NuMA-FLAG was coprecipitated with biotin-wt-pRB, whereas mut-NuMA-FLAG was not detected in the pRB precipitates (Fig. 1C). These results suggest that endogenous pRB binds to NuMA and that their interaction requires the LXCXE motif LSCEE in the C-terminal globular tail of NuMA. Next, we examined the subcellular colocalization of pRB and NuMA during the cell cycle by immunocytochemistry (Fig. 2). The localizations of pRB and NuMA in U2OS cells were exclusively intranuclear during interphase, and they were also largely colocalized during prophase. After prophase, pRB showed diffuse expression throughout the cytosol and NuMA was congregated on the spindle poles. However, a small population of pRB was localized in the vicinity of spindle poles, and yellow merged signals indicating colocalization of pRB and NuMA was detected even after prometaphase.

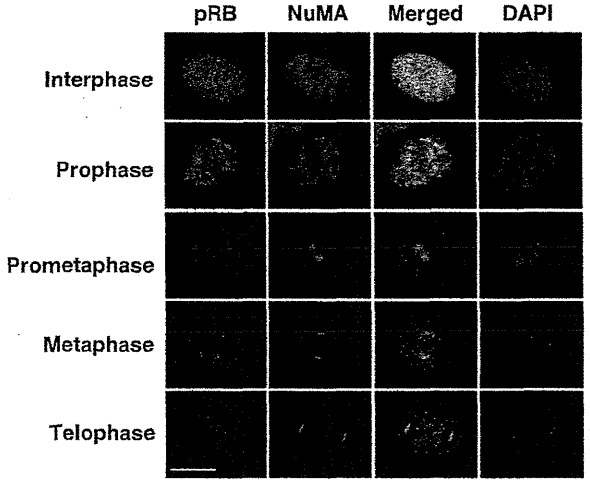

Figure 2 Intracellular localizations of retinoblastoma protein (pRB) and nuclear mitotic apparatus protein (NuMA). Asynchronous U2OS cells were fixed and subjected to immunofluorescence analyses using anti-pRB and anti-NuMA antibodies. Nuclei were stained with DAPI. The bar represents 10 μm.

These data suggest that pRB can interact with NuMA in intact cells during interphase and early M-phase, which may affect the role of NuMA in the organization of spindle microtubules or an unknown function of NuMA in interphase.

siRNA-mediated pRB down-regulation induces abnormal NuMA and spindles

Although the function of NuMA in interphase has not been fully clarified, it is known that nuclear NuMA is multiphosphorylated in the region of amino acids 2000 to 2072 by cyclin B/Cdk1 at the time of nuclear envelope breakdown (NEB) and then translocates to the cytosol to finally congregate in the vicinity of the two centrosomes (Sparks *et al.* 1995; Radulescu & Cleveland 2010). As pRB binding to NuMA requires the LSCEE sequences in the NuMA C-terminal globular tail, which is important for its intracellular localization and association with microtubules, we assumed that pRB inactivation might result in abnormal localization of NuMA and abrogated organization of spindle microtubules.

To investigate whether NuMA function was altered by pRB inactivation, we examined the effects of RB siRNA transfection on the subcellular localization of NuMA and spindle formation in U2OS cells. Knockdown of pRB caused an increase in the number of cells with centrosome hyperamplification, accompanied by the formation of multipolar spindles (Fig. S1 in Supporting information), which often occurs in pRB-inactivated cells, as described previously (Borel *et al.* 2002; Iovino *et al.* 2006). Interestingly, in addition to the multipolar spindle formation, knockdown of pRB induced aberrant alignment of spindle microtubules in metaphase cells, which contained bipolar spindles (Fig. 3A, RB siRNA), whereas the control siRNA had little effect on the spindles (Fig. 3A, control siRNA, and Fig. S1 in Supporting information). Moreover, pRB knockdown resulted in an increase in the number of cells

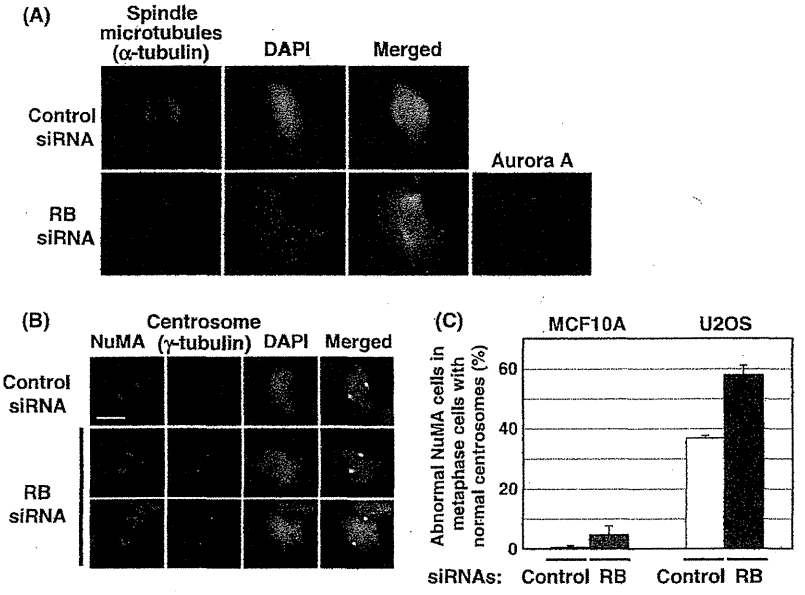

Figure 3 Knockdown of retinoblastoma protein (pRB) induces abnormal alignment of spindle microtubules (A) and distribution of nuclear mitotic apparatus protein (NuMA) (B) with two spindle poles. (A) U2OS cells were transfected with the indicated siRNAs. Endogenous proteins were detected by immunofluorescence analyses (α-tubulin for spindle microtubules; Aurora-A for spindle poles). (B) U2OS cells were transfected with the indicated siRNAs. Endogenous NuMA and centrosomes were detected using antibodies against NuMA and γ-tubulin, respectively. Two different siRNAs for RB were used, and representative images are shown. (C) MCF10A cells and U2OS cells were transfected with the indicated siRNAs and subjected to immunofluorescence analyses as described for (B). The numbers of cells with abnormal NuMA among metaphase cells harboring two centrosomes were counted and normalized by the total number of metaphase cells. The average values with error bars obtained from two different dishes are represented.

expressing abnormally distributed NuMA with two normal centrosomes (Fig. 3B, RB siRNA), whereas the distribution of NuMA was not affected in control cells (Fig. 3B, control siRNA). Abnormal alignment of chromosomes (DAPI staining) was also observed under pRB knockdown. The percentage of U2OS cells with abnormal NuMA but normal number of centrosomes (i.e., 2) among metaphase cells (abnormal NuMA cells) was increased from 37.0% (average) to 57.9% (average) after RB siRNA treatment (Fig. 3C, U2OS). In MCF10A cells, a normal epithelial cell line, RB siRNA treatment increased the percentage of abnormal NuMA cells from 0.6% to 4.6% (Fig. 3C, MCF10A). However, both pRB and NuMA knockdown had no effects on the localizations of NuMA and pRB in interphase, respectively (C. Uchida, unpublished data). In addition, NuMA knockdown did not alter the distribution of pRB in mitotic cells. These results indicate that pRB is required for the proper distribution of NuMA in M-phase cells. Taken together with the finding that the C-terminal LSCEE sequences are important for the interaction of NuMA with pRB, pRB may regulate the mechanism by which NuMA translocates from the nucleus to the centrosomes during G2-phase to early M-phase through binding to the C-terminal of NuMA.

Mut-NuMA-over-expressing cells have abnormal spindles

We further investigated whether over-expression of NuMA could affect the alignment of the spindle microtubules by transient over-expression of wt-NuMA-FLAG or mut-NuMA-FLAG in MCF7 or U2OS cells. wt-NuMA-FLAG was typically localized in the close vicinity of the two centrosomes to form the poles of a symmetric spindle in most of the transfected MCF7 cells (Fig. 4A, wt-NuMA over-expression). Some of the wt-NuMA-FLAG-expressing cells exhibited abnormal distribution of NuMA and misaligned spindle microtubules (C. Uchida, unpublished data). In contrast, abnormal distribution of NuMA and asymmetric alignment of spindle microtubules

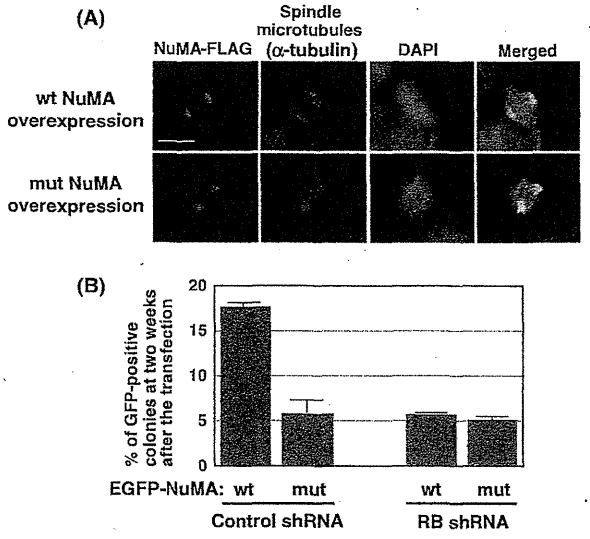

Figure 4 Nuclear mitotic apparatus protein (NuMA)-over-expressing cells have abnormal spindles (A) and low potency for survival (B). (A) MCF7 cells were transfected with expression plasmids for wt-NuMA-FLAG or mut-NuMA-FLAG. NuMA-FLAG and spindle microtubules were detected using antibodies against the FLAG-tag and α-tubulin (Alexa Fluor 488-conjugated), respectively. (B) Wt-NuMA-expressing cells survive for longer periods in the presence of retinoblastoma protein (pRB). U2OS cells were cotransfected with control or RB shRNA vectors and expression vectors for EGFP-wt-NuMA or EGFP-mut-NuMA. The numbers of GFP-positive cell colonies were counted at 2 weeks after transfection. The percentages of EGFP-NuMA colonies among the EGFP-positive colonies in EGFP-transfected cells are shown. The error bars represent the SD.

were often observed in mut-NuMA-FLAG-transfected MCF7 cells (Fig. 4A, mut-NuMA over-expression). The populations of intact mitotic cells were low among U2OS cells over-expressing wt-NuMA-FLAG and mut-NuMA-FLAG (C. Uchida, unpublished data). These results suggest that excess amounts of NuMA or mut-NuMA, which escape from interaction with pRB, can cause defects in the organization of mitotic NuMA and spindles, suggesting an important role of pRB in the NuMA function during M-phase.

Mut-NuMA-over-expressing cells have low potency for survival

It has been shown that abnormal organization of spindles and chromosomes in mitotic cells induces cell death during M-phase, cell cycle arrest, and/or apoptosis in the next cell cycle, owing to failure of mitotic exit or aberrant chromosome reconstitution including micronuclei formation. As we noted that NuMA-FLAG-over-expressing U2OS cells comprised a small population among mitotic cells, we examined the survival rates of wt-NuMA- or mut-NuMA-over-expressing U2OS cells with or without the inhibition of pRB. To perform these examinations, EGFP-wt-NuMA or EGFP-mut-NuMA expression plasmids were cotransfected with shRNA vectors encoding nonrelated sequences (control shRNA) or the 3′UTR of the *RB* sequence (RB shRNA) into U2OS cells and cultured for 2 weeks in the presence of puromycin to select cells with shRNA expression (Fig. S2 in Supporting information).

At 2 days after transfection, abnormal distributions of NuMA in metaphase cells were observed among both EGFP-wt-NuMA- and EGFP-mut-NuMA-expressing cells. Notably, multiple micronuclei also appeared in interphase among EGFP-NuMA-over-expressing cells (Fig. S3 in Supporting information), suggesting that the abnormal mitotic cells could cause aberrant chromosomal segregation and escape from cell death in M-phase to enter the next interphase without complete cytokinesis. However, control cells expressing EGFP did not show any abnormalities in NuMA localization and chromosome organization (C. Uchida, unpublished data). Most of the abnormal cells harboring improper distribution of NuMA and aberrant chromosomes should eventually die by checkpoint-mediated apoptosis or mitotic cell death during several cell cycles. Indeed, 17.7 ± 0.3% and 5.8 ± 1.7% of wt-NuMA- and mut-NuMA-over-expressing cell colonies, respectively, survived, compared with control EGFP-expressing colonies in which pRB was not knocked down (Fig. 4B, control shRNA). Furthermore, the percentage of wt-NuMA-over-expressing colonies declined to 5.7 ± 0.2%, being similar to the percentage of mut-NuMA-over-expressing colonies (5.1 ± 0.5%), under the condition of pRB down-regulation (Fig. 4B, RB shRNA). These results show that wt-NuMA-over-expressing cells can survive for a longer period in the presence of pRB than in the absence of pRB, suggesting an important role of the pRB–NuMA interaction in the regulation of proper cell cycle progression and cell survival.

Discussion

In summary, we found that NuMA is a novel binding partner of pRB and that their interaction is required for the proper distribution of NuMA and organization of spindle microtubules and chromo-

somes in early M-phase. Inactivation of pRB or over-expression of NuMA, particularly pRB-binding-defective NuMA with mutated LXCXE motifs, caused aberrant distribution of NuMA and abnormal spindles. It should be noted that these abnormalities even appeared in cells harboring the normal number of centrosomes/spindle poles, suggesting that centrosome hyperamplification was not the cause of the effects. It remains unclear how pRB can control the proper distribution of NuMA through interaction with the NuMA C-terminal tail containing LSCEE sequences. As pRB and NuMA are predominantly colocalized during interphase and prophase, pRB-NuMA binding may control the timing of Cdk1-mediated phosphorylation of NuMA at NEB. Alternatively, pRB could modify an unknown function of NuMA during interphase, thereby directly or indirectly affecting mitosis.

Although the mechanism for NuMA regulation has not been clarified, this study shows that expression of NuMA that is free from control by pRB, such as over-expressed or mutant NuMA, or down-regulation of pRB, induces abnormal mitotic cells and cell death. Our experimental data suggest that wild-type NuMA in pRB-inactivated or pRB-deficient cells, as well as mutant NuMA with a defect in binding to pRB, tends to be abnormally distributed and misaligned in cytosol, leading to improper organization of spindles. Such cells with abnormal NuMA and spindles eventually proceed to mitotic cell death or apoptosis by checkpoint control in the next cell cycle. However, if some populations of the abnormal cells escape from cell death by abrogation of the checkpoint mechanism, these cells can continue to grow with aberrant chromosomes, which may result in a gain of aneuploidy and chromosomal instability (CIN). CIN is a hallmark in many cancer cells (Sotillo *et al.* 2009; Vitre & Cleveland 2012). During the course of cancer development, CIN is thought to accumulate sufficiently to induce malignant alterations of cells. Indeed, a recent study showed that NuMA is over-expressed in human epithelial ovarian cancer (Bruning-Richardson *et al.* 2012). As the pRB/pRB pathway was also shown to be altered in human high-grade serous epithelial ovarian cancer (Szabova *et al.* 2012), it would be worth considering the linkage between the pRB–NuMA interaction and ovarian cancer development.

LXCXE-containing proteins have been shown to play important roles via cooperation with pRB in nucleosome remodeling, stabilization, and organization of the higher-order structure of chromatin in the regulation of gene expression. NuMA is also assumed to be involved in stabilization of the nuclear matrix and chromatin structure during interphase. From this point of view, it will be interesting to clarify whether pRB-NuMA binding via the LSCEE sequences is required for proper chromatin dynamics during the cell cycle. It is also important to investigate effects of phosphorylation of pRB and NuMA on their interaction. Hyperphosphorylated form of pRB, which is markedly induced by activated Cdks during G1-S phase transition, is known to dissociate from its binding partners including LXCXE proteins as well as chromatin. Assuming that hypophosphorylated form of pRB predominantly binds to NuMA to regulate a certain role in chromatin dynamics during interphase, proper G1-checkpoint could avoid abnormal DNA duplication and mitosis with aberrant chromosomes. In addition, it is reported that chromatin-associated NuMA is hypophosphorylated and phosphorylated NuMA by Cdk1 is released from chromatin. Indeed, intact NuMA was extracted only in a high salt, 0.3–0.42 M NaCl-containing buffer in which it was co-precipitated with pRB (Fig. 1B and C). Notably, a small population of pRB was shown to be colocalized with NuMA even in M-phase (Fig. 2). It is likely that unidentified kinase(s) of pRB in M-phase can control interaction between pRB and NuMA.

Taken together, the findings of this study suggest a unique ability of pRB to regulate the NuMA-mediated alignment of spindle microtubules by controlling an unknown function of NuMA during interphase or directly managing the timing of spindle organization during G2 phase to early M-phase.

Experimental procedures

Cell culture and transfections

MOLT-4 cells were grown in RPMI-1640 medium supplemented with 10% fetal bovine serum (FBS) and 1% penicillin/streptomycin. U2OS cells and MCF7 cells were cultured in DMEM supplemented with 10% FBS and 1% penicillin/streptomycin. MCF10A cells were cultured in MEGM medium (Lonza/Clonetics) supplemented with 100 ng/mL cholera toxin. MCF7-BirA cells were generated by stable expression of BirA, a biotin transferase. The mammalian BirA expression plasmid was kindly provided by Drs D.G. Tenen and A. Kawasaki (CSI-Singapore, National University of Singapore, Singapore). MCF7-BirA cells were cultured in DMEM supplemented with 10% FBS, 300 μg/mL of G418, and 1% penicillin/streptomycin. For transfection of plasmid vectors, cells at 50–60% confluency were transfected using GeneJuice transfection reagent (Merck Millipore) according to the manufacturer's protocol. For transfection of siRNAs, cells were transfected with 10 nM

of the indicated siRNAs using RNAiMAX (Life Technologies) according to the manufacturer's protocol.

Plasmids and siRNA

The wt-NuMA-FLAG expression vector (pTREX-FLAG-NuMA) was kindly provided by Dr M. Enari (National Cancer Center, Tokyo, Japan). A mut-NuMA-FLAG expression vector was generated by mutagenesis using a KOD-Plus-Mutagenesis Kit (Toyobo). EGFP-NuMA expression vectors were generated by subcloning of wt-NuMA or mut-NuMA cDNAs from the corresponding NuMA-FLAG vectors into pEGFP-C1 (Clontech). A Biotin-wt-RB plasmid vector (pCMV5-Biot-wt-RB) was generated by subcloning of biotinylation signal sequences into pCMV5-wt-RB. The RB sequences targeted by the siRNAs were 5′-CUUGACAAGAGAAAUGAUA-3′ and 5′-CCAUGCUUAAAUCAGAAGA-3′. The sequence of the control siRNA was 5′-UUCUCCGAACGUGUCACGU-3′. Control (pLKO.1-puro-nontarget shRNA) and RB (pLKO.1-puro-RB shRNA, TRCN0000010419) shRNA vectors were purchased from Sigma-Aldrich.

Antibodies

The following antibodies were used: anti-pRB (G3-245; BD Biosciences); anti-NuMA (Novus); anti-FLAG (M2; Sigma); anti-α-tubulin (DM1A; Sigma); Alexa Fluor 488-conjugated anti-α-tubulin (EXBIO); anti-γ-tubulin (GTU-88; Sigma); anti-Aurora-A (IHC; Bethyl Laboratories); Alexa Fluor 488-conjugated anti-mouse IgG; and Alexa Fluor 568-conjugated anti-rabbit IgG (Life Technologies).

Immunoprecipitation and Western blotting

MOLT-4 cells were lysed in lysis buffer [25 mM Tris-HCl pH 7.4, 0.5% NP-40, 0.15 M NaCl, 1 × Halt protease inhibitor cocktail (Thermo Scientific)]. The lysates were centrifuged at 5000 *g* for 5 min at 4 °C, and the pellets were resuspended in a high salt buffer (25 mM Tris-HCl, pH 7.4, 0.5% Triton X-100, 0.42 M NaCl, 1 × Halt protease inhibitor cocktail) on ice for 5 min. The suspensions were centrifuged at 12 000 *g* for 15 min at 4 °C. The supernatants were diluted by three-fold in PBS(-) and centrifuged at 10 000 *g* for 5 min at 4 °C. The supernatants were incubated with anti-pRB (G3-245) or anti-NuMA antibodies for 2 h at 4 °C with gentle rotation. After subsequent incubation of the lysates with Dynabeads Protein G (Life Technologies) at 4 °C with gentle rotation, the Dynabeads were precipitated and washed three times with lysis buffer using a Dynabeads magnetic rack. The bound proteins were eluted with SDS-sample buffer and subjected to SDS-PAGE, followed by transfer to a PVDF membrane. After blocking with 5% skim milk in PBS(-) containing 0.1% Tween 20 (PBS-T) at room temperature for 1 h, the membrane was incubated with the primary antibodies against pRB or NuMA diluted in 5% skim milk in PBS-T at room temperature for 1 h. Following three washes with PBS-T, the membrane was incubated in 5% skim milk in PBS-T containing a horseradish peroxidase-conjugated secondary antibody. After washing, the bound antibody signals were detected using the SuperSignal West Pico Substrate (Thermo Scientific).

For pull-down of biotinylated pRB from MCF7-BirA cells transfected with pCMV5-Biot-wt-RB and pTREX-FLAG-NuMA, cell lysates were prepared using PD buffer (25 mM Tris-HCl pH 7.4, 0.5% Triton X-100, 0.3 M NaCl, 1 × Halt protease inhibitor cocktail). The lysates were incubated with Dynabeads streptavidin for 2 h at 4 °C with gentle rotation, followed by precipitation and washing with PD buffer using a Dynabeads magnetic rack. The bound proteins were analyzed by Western blotting as described above using anti-FLAG and anti-pRB antibodies.

Immunofluorescence analysis

For the experiments shown in Fig. 2, cells were plated on 35-mm glass-bottom dishes. On the following day, the cells were fixed in methanol for 20 min at −20 °C. After removing the methanol, the cells were incubated in 4% paraformaldehyde at room temperature for 15 min, permeabilized with 0.2% Triton X-100 in PBS(-) for 5 min, and blocked with 5% FBS in PBS(-) for 1 h at room temperature. The cells were then incubated with primary antibodies diluted 1:100–1:200 in 1% FBS overnight at 4 °C, washed with PBS(-), and incubated with Alexa Fluor 488- or 568-conjugated secondary antibodies. Fluorescent images were obtained using an FV1000 laser scanning microscope (Olympus). For the experiments shown in Figs 3 and 4, cells were plated on 2–3 pieces of 8-well Lab-Tek II chamber slides (Nalge Nunc). Transfections were carried out on the following day, and immunostaining was carried out at 2 days after transfection as described above. Fluorescent images were obtained using an IX73 microscope (Olympus). For the experiments shown in Fig. 4B, cells were plated on 6-cm dishes and transfected with plasmids on the following day. At 2 days after transfection, the cells were detached and reseeded at the same number in each well of the chamber slides. The cell culture was then continued for 2 weeks in the presence of 1 μg/mL puromycin. Fluorescent images were obtained using an IX73 microscope (Olympus).

Acknowledgements

We thank Daniel G Tenèn and Akira Kawasaki for providing a BirA expression plasmid, and Masato Enari for providing pTREX-FLAG-NuMA. This work was supported by core grant of the Cancer Science Institute, National University of Singapore.

References

Alderton, G.K. (2010) Genome instability: RB moonlights in mitosis. *Nat. Rev. Mol. Cell Biol.* **11**, 541.

Borel, F., Lohez, O.D., Lacroix, F.B. & Margolis, R.L. (2002) Multiple centrosomes arise from tetraploidy checkpoint failure and mitotic centrosome clusters in p53 and RB pocket protein-compromised cells. *Proc. Natl Acad. Sci. USA* **99**, 9819–9824.

Bruning-Richardson, A., Bond, J., Alsiary, R., Richardson, J., Cairns, D.A., McCormac, L., Hutson, R., Burns, P.A., Wilkinson, N., Hall, G.D., Morrison, E.E. & Bell, S.M. (2012) NuMA overexpression in epithelial ovarian cancer. *PLoS ONE* **7**, e38945.

Chan, H.M., Smith, L. & La Thangue, N.B. (2001) Role of LXCXE motif-dependent interactions in the activity of the retinoblastoma protein. *Oncogene* **20**, 6152–6163.

Dahiya, A., Gavin, M.R., Luo, R.X. & Dean, D.C. (2000) Role of the LXCXE binding site in Rb function. *Mol. Cell. Biol.* **20**, 6799–6805.

van Deursen, J.M. (2007) Rb loss causes cancer by driving mitosis mad. *Cancer Cell* **11**, 1–3.

Dyson, N. (1998) The regulation of E2F by pRB-family proteins. *Genes Dev.* **12**, 2245–2262.

Endo, A., Moyori, A., Kobayashi, A. & Wong, R.W. (2013) Nuclear mitotic apparatus protein, NuMA, modulates p53-mediated transcription in cancer cells. *Cell Death Dis.* **4**, e713.

Iovino, F., Lentini, L., Amato, A. & Di Leonardo, A. (2006) RB acute loss induces centrosome amplification and aneuploidy in murine primary fibroblasts. *Mol. Cancer* **5**, 38.

Itoh, G., Sugino, S., Ikeda, M., Mizuguchi, M., Kanno, S., Amin, M.A., Iemura, K., Yasui, A., Hirota, T. & Tanaka, K. (2013) Nucleoporin Nup188 is required for chromosome alignment in mitosis. *Cancer Sci.* **104**, 871–879.

Manning, A.L., Longworth, M.S. & Dyson, N.J. (2010) Loss of pRB causes centromere dysfunction and chromosomal instability. *Genes Dev.* **24**, 1364–1376.

Ohata, H., Miyazaki, M., Otomo, R., Matsushima-Hibiya, Y., Otsubo, C., Nagase, T., Arakawa, H., Yokota, J., Nakagama, H., Taya, Y. & Enari, M. (2013) NuMA is required for the selective induction of p53 target genes. *Mol. Cell. Biol.* **33**, 2447–2457.

Radulescu, A.E. & Cleveland, D.W. (2010) NuMA after 30 years: the matrix revisited. *Trends Cell Biol.* **20**, 214–222.

Schvartzman, J.M., Duijf, P.H., Sotillo, R., Coker, C. & Benezra, R. (2011) Mad2 is a critical mediator of the chromosome instability observed upon Rb and p53 pathway inhibition. *Cancer Cell* **19**, 701–714.

Sotillo, R., Schvartzman, J.M. & Benezra, R. (2009) Very CIN-ful: whole chromosome instability promotes tumor suppressor loss of heterozygosity. *Cancer Cell* **16**, 451–452.

Sparks, C.A., Fey, E.G., Vidair, C.A. & Doxsey, S.J. (1995) Phosphorylation of NUMA occurs during nuclear breakdown and not mitotic spindle assembly. *J. Cell Sci.* **108**(Pt 11), 3389–3396.

Szabova, L., Yin, C., Bupp, S., Guerin, T.M., Schlomer, J.J., Householder, D.B., Baran, M.L., Yi, M., Song, Y., Sun, W., McDunn, J.E., Martin, P.L., Van Dyke, T. & Difilippantonio, S. (2012) Perturbation of Rb, p53, and Brca1 or Brca2 cooperate in inducing metastatic serous epithelial ovarian cancer. *Cancer Res.* **72**, 4141–4153.

Uchida, C. (2012) The retinoblastoma protein: functions beyond the G1-S regulator. *Curr. Drug Targets* **13**, 1622–1632.

Vitre, B.D. & Cleveland, D.W. (2012) Centrosomes, chromosome instability (CIN) and aneuploidy. *Curr. Opin. Cell Biol.* **24**, 809–815.

Wong, R.W., Blobel, G. & Coutavas, E. (2006) Rae1 interaction with NuMA is required for bipolar spindle formation. *Proc. Natl Acad. Sci. USA* **103**, 19783–19787.

Received: 25 September 2013
Accepted: 15 October 2013

Supporting Information

Additional Supporting Information may be found in the online version of this article at the publisher's web site:

Figure S1 Downregulation of pRB induces multipolar spindles caused by centrosome hyperamplification.

Figure S2 Evaluation of the RB shRNA.

Figure S3 Overexpression of NuMA induces abnormal distribution of NuMA and multiple micro nuclei.

International Journal of Cancer

Anti-VEGF antibody therapy induces tumor hypoxia and stanniocalcin 2 expression and potentiates growth of human colon cancer xenografts

Shinichiro Miyazaki[1], Hirotoshi Kikuchi[1], Ichirota Iino[1], Takashi Uehara[1], Tomohiko Setoguchi[1], Takeshi Fujita[1], Yoshihiro Hiramatsu[1], Manabu Ohta[2], Kinji Kamiya[1], Kyoko Kitagawa[3], Masatoshi Kitagawa[3], Satoshi Baba[4] and Hiroyuki Konno[1]

[1] Second Department of Surgery, Hamamatsu University School of Medicine, Hamamatsu, Japan
[2] Oncology Center, Hamamatsu University School of Medicine, Hamamatsu, Japan
[3] Department of Molecular Biology, Hamamatsu University School of Medicine, Hamamatsu, Japan
[4] Department of Pathology, Hamamatsu University School of Medicine, Hamamatsu, Japan

Tumor angiogenesis plays a critical role in colorectal cancer progression. Recent randomized clinical trials have revealed the additive effect of bevacizumab, a humanized monoclonal antibody against vascular endothelial growth factor (VEGF)-A, to conventional chemotherapy in the improved survival of patients with metastatic colorectal cancer. However, a number of preclinical reports indicate the development of resistance to anti-angiogenic therapy. In this study, we addressed the effects of anti-VEGF antibodies on the growth and malignant behavior of colorectal cancer cells. TK-4, a solid tumor strain derived from a colon cancer patient, was subcutaneously or orthotopically implanted into nude mice. Short-term administration of anti-VEGF antibodies inhibited the growth of cecal tumors at day 14 by suppressing mitosis, but prolonged treatment resulted in the recovery of cellular proliferation and suppression of apoptosis at day 35. Intratumoral hypoxia induced by anti-VEGF antibody treatment resulted in activation of hypoxia inducible factor-1α protein and an increased number of aldehyde dehydrogenase 1-positive tumor cells. In microarray analysis, *stanniocalcin 2* (STC2) was the most highly upregulated gene in anti-VEGF antibody-treated tumors. *In vitro* analyses showed that the growth and migration of SW480 colon cancer cells under hypoxic conditions were significantly inhibited by knockdown of STC2. *In vivo* serial transplantation of TK-4 revealed that long-term administration of anti-VEGF antibodies increased the tumorigenicity of colon cancers and accelerated tumor growth when transplanted into secondary recipient mice. Our data provide a potential molecular explanation for the limited clinical effectiveness of anti-VEGF antibodies.

Cancer Cell Biology

Colorectal cancer is a leading cause of cancer death in the developed world.[1] Patients who die of colorectal cancer suffer from advanced disease that is refractory to systemic therapy. Angiogenesis is necessary for the growth of colorectal cancer and metastasis to secondary organs,[2] whereas other malignant tumors can grow without angiogenesis.[3] The idea of targeting angiogenesis in malignant tumors was pioneered by Judah Folkman. A randomized clinical trial revealed that the addition of bevacizumab, a humanized monoclonal antibody against vascular endothelial growth factor (VEGF)-A, to conventional chemotherapy prolonged survival in patients with metastatic colorectal cancer compared with chemotherapy alone.[4] Since then, various anti-angiogenic agents such as anti-VEGF receptor antibodies, soluble VEGF receptor and VEGF receptor tyrosine kinase inhibitor have been developed.[5,6] However, preclinical observations revealed the emergence of resistance to anti-angiogenic therapy in several tumor models.[7–9] Notably, it has been reported that withdrawal of bevacizumab accelerated tumor regrowth in patients with colorectal cancer.[10] In contrast, retrospective pooled analysis of five placebo-controlled clinical trials revealed that cessation of bevacizumab therapy did not alter the disease progression pattern.[11] Bevacizumab is frequently utilized in advanced colorectal cancer[12]; however, the molecular events occurring during anti-angiogenic therapy that may or may not mediate resistance to therapy in colorectal cancer remain to be elucidated. In this study, we sought to define the effects of anti-VEGF antibodies on the tumor

Key words: colon cancers, angiogenesis, VEGF, hypoxia, stanniocalcin 2
Additional Supporting Information may be found in the online version of this article.
Grant sponsor: Ministry of Education, Culture, Sports, Science and Technology of Japan Grants-in-aid; **Grant number(s):** 22791270, 24591937, 22300329, 24390312
DOI: 10.1002/ijc.28686
History: Received 30 July 2013; Accepted 10 Dec 2013; Online 20 Dec 2013
Correspondence to: Hirotoshi Kikuchi, Second Department of Surgery, Hamamatsu University School of Medicine, 1-20-1 Handayama, Higashi-ku, Hamamatsu 431-3192, Japan, Tel.: +[81-53-435-2279], Fax: +[81-53-435-2273], E-mail: kikuchih@hama-med.ac.jp

What's new?

Antibodies against vascular endothelial growth factor (VEGF) are used in the treatment of colorectal cancer, but tumors may become resistant to them. In this study, anti-VEGF antibodies were found to effectively suppress the growth of cecal tumors at day 14 in a colorectal cancer xenograft mouse model. At day 35, however, indications of drug resistance emerged. Intratumoral hypoxia induced by treatment played an important role in regulating multiple processes that accelerated the malignant potential of colon cancers. The data may explain the molecular mechanism behind the limited clinical effectiveness of anti-VEGF antibodies.

microenvironment as well as on the growth and malignant behavior of human colon cancer xenografts.

Material and Methods

Animal experiments

Experiments were performed according to the guidelines of the Committee on Experimental Animals of Hamamatsu University School of Medicine. Mouse monoclonal anti-human VEGF antibodies (clone26503, R&D Systems, Minneapolis, MN), mouse monoclonal IgG2B isotype control (clone133303, R&D Systems) and IgG (human purified antigen lyophilized, MP Biomedicals, Solon, OH) were purchased. Bevacizumab was provided by Chugai Pharmaceutical Co, Tokyo, Japan. *In vivo* experiments were conducted using a patient-derived xenograft (PDX) model. TK-4 is a solid tumor tissue strain, which was derived from a human colon carcinoma obtained from a surgically resected specimen at our institution. TK-4 was subcutaneously implanted into the bilateral axillary regions or orthotopically implanted into the cecal walls of 6-week-old male BALB/c nu/nu mice (CLEA Japan, Tokyo, Japan) by suturing 100 mm^3 tumor pieces with 6-0 Polysorb (Tyco Healthcare, Schaffhausen, Switzerland) as previously described.[13–16] Tumors were measured with calipers and tumor volume was calculated as: tumor volume (mm^3) = $\pi\times$ length (mm) $\times$ width (mm) $\times$ height (mm)/6.

Treatment protocol 1

TK-4 was orthotopically implanted and mice were intraperitoneally treated with anti-human VEGF antibodies or IgG2B isotype control (25 μg/body/day, three times per week; $n = 14$) from day 7 after orthotopic implantation (Supporting Information Fig. S1a, b). After 14 and 35 days of treatment, mice were sacrificed and tumors were removed ($n = 4$ and $n = 10$ for the treated and control groups, respectively; Supporting Information Fig. S1a).

Treatment protocol 2

TK-4 was subcutaneously implanted into 6-week-old mice as described earlier. From day 7 after implantation, bevacizumab or control IgG ($n = 35$) was intraperitoneally administered to tumor-bearing mice at 5 mg/kg/day twice a week. After 28, 56 and 84 days from antibody administration, 10, 10 and 15 bevacizumab-treated and control mice, respectively, were sacrificed and tumors were removed. Tumors were cut into sections of equal size (100 mm^3) and orthotopically implanted into the cecal walls of secondary recipient mice (groups A, B and C, Supporting Information Fig. S2). Eight weeks after tumor transplantation, mice were sacrificed and tumors were removed. All tumor samples were fixed in formalin or treated with RNAlater (Applied Biosystems, Grand Island, NY) for further analyses.

Cell cultures

SW480 cells were provided by Dr. Keiichi Nakayama (Kyushu University, Fukuoka, Japan), and tested and authenticated by the National Institute of Biomedical Innovation (Osaka, Japan). The HCT116 cells were purchased from the American Type Culture Collection. Cells were maintained in Dulbecco's modified Eagle's medium (DMEM) supplemented with 10% fetal bovine serum (FBS). Hypoxic conditions were achieved by culturing cell lines in a sealed hypoxia chamber (Billups-Rothenberg, Del Mar, CA) after flushing with a mixture of 1% O_2 and 5% CO_2 balanced with N_2, as described previously.[17]

Patient characteristics and tissue specimens

Formalin-fixed paraffin-embedded tissues of colorectal liver metastasis from 14 Japanese patients who underwent hepatectomy at the Second Department of Surgery, Hamamatsu University School of Medicine between May 2007 and November 2013 were utilized for histological and immunohistochemical analyses. Of the 14 patients, 10 received conventional chemotherapy alone and four received conventional chemotherapy in combination with bevacizumab before hepatectomy. The study was performed in accordance with the guidelines for pathological specimen handling, which was approved by the ethical committee of the Hamamatsu University School of Medicine. Patients' characteristics are shown in Supporting Information Table S3.

Histological examinations

To evaluate mitotic index, the number of mitotic cells and the total number of tumor cells were counted in five high-power fields (HPFs) of hematoxylin and eosin (H&E)-stained tumor sections using a light microscope under $\times$400 magnification. Mitotic index was calculated as: mitotic index (%) = mitotic cells/total tumor cells $\times$100. To quantify necrotic areas of human colorectal liver metastases,

photographic images of H&E-stained sections were captured and image analysis was performed using ImageJ software (NIH). The necrotic area was calculated as: necrotic area (%) = pixels of necrotic area/pixels of total tumor area × 100.

TUNEL assay

Terminal deoxynucleotidyl transferase-mediated dUTP nick-end labeling (TUNEL) assays were performed to determine apoptotic cells. The procedure was carried out using an in situ apoptosis detection kit (TaKaRa Bio, Shiga, Japan). Briefly, after deparaffinization, sections were treated with 20 μg/ml proteinase K for 10 min. After treatment with 3% H_2O_2 in methanol for 10 min, sections were incubated with TUNEL reaction mixture for 70 min at 37°C. Further incubation with anti-fluorescein isothiocyanate–horseradish peroxidase conjugate was performed for 30 min at 37°C. Sections were stained with diaminobenzidine solution for 10 min at room temperature and then counterstained with 2% methyl green. The nuclei of apoptotic cells were labeled brown with diaminobenzidine staining. The number of TUNEL-positive cells and the total number of tumor cells in five HPFs from each tumor specimen were counted using a light microscope under ×400 magnification.

Microarray analysis

Total RNA was extracted from frozen tumor specimens using an RNeasy Mini Kit (Qiagen, Valencia, CA). The expression profiles of anti-human VEGF antibody-treated tumors and control tumors were determined using an Affymetrix oligonucleotide microarray (Human Gene 1.0 ST Array) according to the manufacturer's protocol. Three chips per group were hybridized. To focus on groups of genes that share common biological function, gene set enrichment analysis software (Broad Institute of Massachusetts Institute of Technology and Harvard University, http://www.broad.mit.edu/gsea) was utilized. The gene sets database- c2.cgp.v2.5.symbols.gmt (curated) was used. All gene sets with more than 500 genes or fewer than 15 genes were automatically excluded, according to the default settings. The difference between signal-to-noise ratios was used as the association score. The number of phenotype permutations involved in the nominal *p*-value calculation was 1,000. The gene sets with false discovery rates of <25% or nominal *p*-values of <0.01 were defined as significant. GeneSpringGX11 software (Agilent, Santa Clara, CA) was used to identify candidate genes and changes in gene expression of >1.18-fold were determined as significant. Normalized microarray data were deposited at the Gene Expression Omnibus (accession number GSE47087).

Quantitative real-time PCR analysis

Total RNA was extracted from tumor tissues and cultured cells as described above and reverse transcription was performed using a PrimerScript RT Reagent Kit (TaKaRa Bio). The resulting cDNA was amplified by real-time PCR using the Rotor-Gene RG3000 Real-time PCR Detection System (Corbett Research, Mortlake, Australia) and SYBR Premix Ex Taq (TaKaRa Bio). Primer sequences were: 5′-GCCATCAGG GAAATGGTGTC-3′ and 5′-AGGTCAGCAGCAAGTTCAC G-3′ for human stanniocalcin 2 (STC2) and 5′-AGAAGGAT TCCTATGTGGGC-3′ and 5′-ATAGCACAGCCTGGATAG CA-3′ for human β-actin (ACTB).

Immunohistochemical analysis

For immunohistochemical analyses of CD31, hypoxia inducible factor (HIF)-1α, STC2 and aldehyde dehydrogenase1 (ALDH1), 4-μm-thick sections from formalin-fixed paraffin-embedded tissues were used. Tumor sections were deparaffinized with sequential xylene and ethanol treatment, as well as rehydration. Antigen retrieval was conducted by heating the samples at 95°C for 40 min in pH 9 Tris/EDTA buffer for STC2 and ALDH1, at 120°C for 15 min in pH 6 sodium citrate buffer for HIF-1α or at 95°C for 40 min in pH 6 sodium citrate buffer for CD31. Slides were rinsed with phosphate-buffered saline (PBS) and incubated with 3% H_2O_2 in absolute methanol for 15 min to quench endogenous peroxidase activity. After a further washing step with PBS, anti-mouse CD31 antibodies (1:200; Abcam, Cambridge, UK), anti-human HIF-1α antibodies (1:500; Novus, Littleton, CO), anti-human STC2 antibodies (1:50; Abcam for xenografts, and 1:50; Abnova, Taipei, Taiwan for human clinical specimens) and anti-human ALDH1 antibodies (1:200; Abcam) were applied. Immunocomplexes were detected using Simple Stain Universal Reagent (Nichirei, Tokyo, Japan) and diaminobenzidine. The sections were lightly counterstained with hematoxylin and mounted with a permanent mounting medium.

Microvessel density was scored from CD31-stained sections using a light microscope under ×400 magnification in five HPFs, according to the previous reports by Weidner *et al.*[18] Briefly, large microvessels and single brown-staining endothelial cells clearly separated from adjacent microvessels, tumor cells, and other connective tissue elements were considered a single, countable microvessel. Branching structures were counted as one, unless there was a break in the continuity of the vessel in which case it was counted as two distinct vessels. To evaluate the ratio of HIF-1α nuclear positivity, nuclear positive cells and total tumor cells were counted. To evaluate the ratio of ALDH1 positivity, ALDH1-positive cells and total tumor cells were counted. For the evaluation of STC2 expression, the staining intensity of STC2 was scored as 0 (none), 1+ (weak), 2+ (moderate) or 3+ (strong). All images were obtained using a light microscope at ×400 magnification. Five HPFs from each tumor specimen were evaluated using ImageJ software (NIH).

Quantitation of stromal area in mice xenografts

Subcutaneous tumors in treatment protocol 2 were stained with Masson's trichrome and photographic images were captured under a light microscope at ×100 magnification. Image

analysis was performed to quantify the stromal area in five fields for each specimen using Adobe Photoshop software.[19] The stromal area was calculated as: stromal area (%) = pixels of green area/pixels of total area × 100.

RNA interference

Cells were transfected with 20 nmol/l stealth small interfering RNA (siRNA) duplex oligos using Lipofectamine RNAiMAX (Invitrogen, Carlsbad, CA) according to the manufacturer's instructions. Nucleotide sequences of siRNAs were as follows: STC2 #1, 5′-r(GGCUUACAUGGGAUUUGCAUGACUU)d(TT)-3′; for STC2 #2, 5′-r(GGGUGAUAGUGGAGAUGAUCCAUUU)d(TT)-3′; HIF-1α #1, 5′-r(AGUUCCAGUGACUCUGGAU)d(TT)-3′ and HIF-1α #2, 5′-r(AUGGAACAUGAUGGUUCAC)d(TT)-3′. Stealth RNAi Negative Control Medium GC Duplex (Invitrogen) was used as the control.

Western blot

Cells were lysed in chilled lysis buffer supplemented with a complete protease inhibitor cocktail (Roche, Basel, Switzerland). Protein extracts (50 μg) were subjected to 10% PAGE followed by electroblotting onto Immobilon-P polyvinylidene fluoride membrane (Millipore, Billerica, MA). Blots were probed with mouse monoclonal anti-STC2 (1:5,000, Novus), mouse monoclonal anti-HIF-1α (1:500, BD Bioscience, San Jose, CA), and anti-β-actin (1:500,000, Sigma, St. Louis, MO) antibodies. Immunoreactive proteins were visualized using Western Lighting Chemiluminescence Reagent Plus (Perkin–Elmer, Waltham, MA).

Cell counting assay

The growth of SW480 cells was assessed by cell counting. Briefly, cells were seeded in a 12-well plate at a density of 1×10^4 cells/well in DMEM supplemented with 10% FBS and allowed to adhere for 24 hr before the assay. Cells were transfected with oligonucleotides as described above and cultured at 37°C for 36 hr before the plates were transferred into the indicated conditions. After 0 (starting point), 24, 48 and 72 hr of incubation, the cells were detached using trypsin-EDTA solution and counted on a hemocytometer. Dead cells were excluded using Trypan blue (GIBCO, Grand Island, NY). Cell growth is defined as the cell count percentage increase, calculated as: cell count % increase = cell count (each time point)/cell count at 0 hr (starting point) × 100.

Scratch assay

The migration of SW480 cells was assessed by scratch assay. Briefly, cells were seeded in a four-well chamber slide (Thermo Scientific, Boston, MA) at a density of 1×10^5 cells/well in DMEM with 10% FBS, then transfection and cultures were performed in the same manner as that for the cell counting assay. After culturing at 37°C for 36 hr, scratches were made on the slides using a sterile 200-μl pipette tip before the slides were incubated under the indicated conditions over the next 48 hr. Photographs were taken to monitor closure of the gap using a light microscope. Wound closure was evaluated using ImageJ software and calculated as follows: % wound closure = (area of gap (0 hr) − area of gap (48 hr))/area of gap (0 hr) × 100.

Statistical analysis

Data are presented as mean ± SE. Statistical significance of differences were assessed using a student's *t* test or Mann Whitney's U test. A *p*-value of <0.05 was considered statistically significant.

Results

Treatment with anti-VEGF antibodies inhibits growth of orthotopic human colon cancer xenografts

To determine whether treatment with anti-VEGF antibodies influences the characteristics of colorectal cancer *in vivo*, TK-4 human colon cancer xenografts were orthotopically implanted into the cecal walls of nude mice, and mice were treated with anti-human VEGF antibodies or control IgG (Supporting Information Fig. S1a, b). After 14 and 35 days of treatment, mice were sacrificed and cecal tumors were resected (Supporting Information Fig. S1a). Tumor volume and weight were significantly lower in anti-VEGF antibody-treated mice (487.9 ± 247.3 mm^3 and 0.58 ± 0.27 g) than control mice (968.5 ± 492.5 mm^3 and 1.01 ± 0.45 g) at day 35 ($p = 0.012$ and $p = 0.017$) (Figs. 1*a* and 1*b*). Immunohistochemical analysis for CD31, an endothelial specific marker, revealed a significant decrease in microvessel density in anti-VEGF antibody-treated tumors (control *vs.* anti-VEGF; 18.32 *vs.* 8.96 vessels/HPF, $p < 0.01$) (Fig. 1*c*). In contrast, no difference was observed in body weights between the two groups (Supporting Information Fig. S1c). These results suggest that anti-VEGF antibodies inhibited angiogenesis, as well as growth of colon cancer xenografts with minimal systemic effects in mice.

Treatment with anti-VEGF antibodies temporarily suppresses mitosis of tumor cells and prolonged treatment suppresses apoptosis

It has recently been noted that continuous treatment with anti-VEGFR2 antibodies or sunitinib, a multi-kinase inhibitor, increased the malignant potential of pancreatic islet tumors and breast cancers.[8,9] To investigate whether a similar phenotypic alteration occurred during anti-VEGF antibody therapy in our orthotopic implantation model of a human colon cancer xenograft, mitosis and apoptosis were evaluated in tumor specimens at days 14 and 35. Although the mitotic index was significantly lower in anti-VEGF antibody-treated tumors compared with the control at day 14 (control *vs.* anti-VEGF; 3.56 *vs.* 2.72%, $p = 0.040$), it was comparable at day 35 (Fig. 1*d*). In contrast, the ratio of apoptotic cells in anti-VEGF antibody-treated tumors was significantly lower than in the control at day 35 (control *vs.* anti-VEGF; 2.23 *vs.* 1.64/HPF, $p < 0.01$), whereas it was equivalent to the control at day 14 (Fig. 1*e*). These data suggest that short term

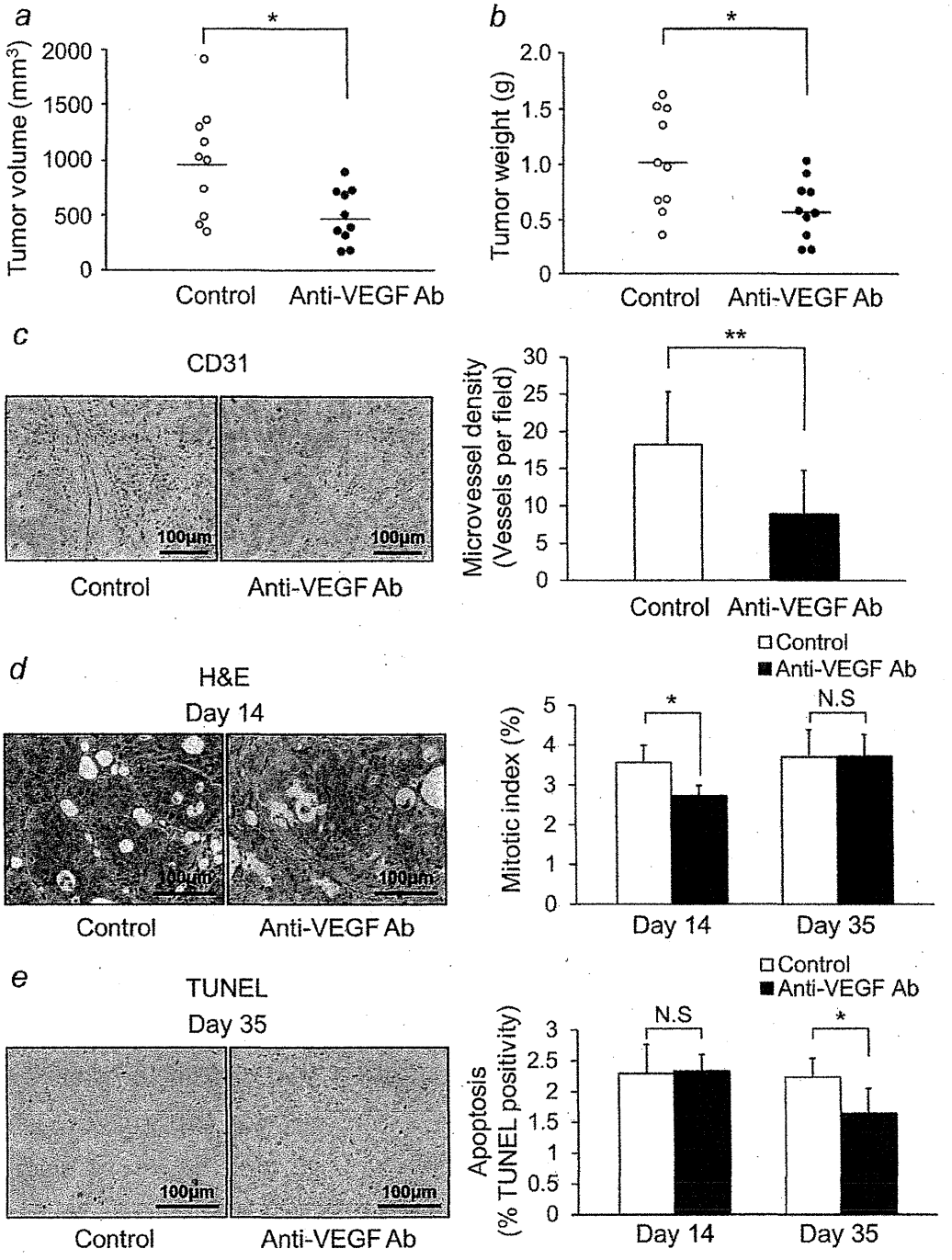

Figure 1. Effects of anti-VEGF antibody therapy on growth and angiogenesis of orthotopic human colon cancer xenografts. TK-4, a solid tumor strain derived from a colon cancer patient, was orthotopically implanted into the cecal walls of nude mice and treated with anti-VEGF antibodies or control IgG for 35 days. (*a*) Tumor volume was significantly lower in anti-VEGF antibody-treated mice (487.9 ± 247.3 mm^3) than control mice (968.5 ± 492.5 mm^3) ($p = 0.012$). (*b*) Tumor weights were significantly lower in anti-VEGF antibody-treated mice (0.58 ± 0.27 g) than control mice (1.01 ± 0.45 g) ($p = 0.017$). (*c*) Immunohistochemical analysis for CD31 in cecal tumors. *Left*, representative images of CD31 staining at day 35 (endothelial cells; ×400 magnification); *right*, quantitative evaluation of microvessel density (average of five high-power fields) in control and anti-VEGF antibody-treated mice. Microvessel density was significantly lower in anti-VEGF antibody-treated tumors (8.96 vessels/high-power field) than in control tumors (18.32 vessels/high-power field) ($p < 0.01$). (*d*) Histologic examination for mitoticindex. *Left*, representative images of H&E staining at day 14 (×400 magnification); *right*, quantitative evaluation of tumor cell mitotic index (average of five high-power fields) at day 14 ($n = 4$, for each group) and at day 35 ($n = 10$, for each group). Mitotic indexes were significantly lower in anti-VEGF antibody-treated tumors (2.72%) compared with the control (3.56%) at day 14 ($p = 0.040$) and were comparable at day 35. (*e*) Histologic examination for apoptotic cells. *Left*, representative images of TUNEL assays at day 35 (×400 magnification); *right*, quantitative evaluation of TUNEL positive ratios in tumor cells (average of five high-power fields) at days 14 ($n = 4$, for each group) and 35 ($n = 10$, for each group). Ratios of apoptotic cells in anti-VEGF antibody-treated tumors were significantly lower (1.64%) than that of the control (2.23%) at day 35 ($p < 0.01$), whereas it was equivalent to the control at day 14. Bars, SE; *, $p < 0.05$; **, $p < 0.01$; N.S, not significant.